

METHODS ARTICLE

Development of an Advanced Primary Human *In Vitro* Model of the Small Intestine

Matthias Schweinlin,¹ Sabine Wilhelm,¹ Ivo Schwedhelm,¹ Jan Hansmann, PhD,¹ Rene Rietscher, PhD,² Christian Jurowich, MD,³ Heike Walles, PhD,^{1,4} and Marco Metzger, PhD^{1,4}

Intestinal *in vitro* models are valuable tools in drug discovery and infection research. Despite several advantages, the standard cell line-based Transwell[®] models based for example on colonic epithelial Caco-2 cells, lack the cellular complexity and transport activity associated with native small intestinal tissue. An additional experimental set-back arises from the most commonly used synthetic membranes, on which the cells are routinely cultured. These can lead to an additional barrier activity during *in vitro* testing. To overcome these limitations, we developed an alternative primary human small intestinal tissue model. This novel approach combines previously established gut organoid technology with a natural extracellular matrix (ECM) based on porcine small intestinal scaffold (SIS). Intestinal crypts from healthy human small intestine were expanded as gut organoids and seeded as single cells on SIS in a standardized Transwell-like setting. After only 7 days on the ECM scaffold, the primary cells formed an epithelial barrier while a subpopulation differentiated into intestinal specific cell types such as mucus-producing goblet cells or hormone-secreting enteroendocrine cells. Furthermore, we tested the influence of subepithelial fibroblasts and dynamic culture conditions on epithelial barrier function. The barrier integrity was stabilized by coculture in the presence of gut-derived fibroblasts. Compared to static or dynamic culture on an orbital shaker, dynamic culture in a defined perfusion bioreactor had an additional significant impact on epithelial cell differentiation, indicated by high prismatic cell morphology and upregulation of CYP3A4 enzyme and Mdr1 transporter activity. In summary, more physiological tissue models as presented in our study might be useful tools in preclinical research and development.

Introduction

IN THE HUMAN BODY, the small intestine represents the organ exhibiting the largest contact surface to the environment. Thus, most of the food digestion and absorption of nutrients takes place in this highly specialized organ. The intestinal mucosa has to function as a tight barrier between the gut and the intestinal lumen to keep out invading microorganisms while retaining absorptive function. Key players in this barrier function are the intestinal epithelial cells (IECs) by controlling the passage of ions and molecules and thereby being critical for intestinal homeostasis.^{1,2} Both the barrier function and epithelial metabolism are strongly dependent on paracrine and exogenous factors, and on extracellular matrix (ECM) components and epithelial–mesenchymal cell–cell interactions within the intestinal mucosa.

Mimicking the natural microenvironment in the gut leads to more physiological and predictive *in vitro* models, which may

help to reduce animal experimentation and to counteract the rising failure rates in mandatory phase of clinical trials. The most widely used *in vitro* test systems rely on immortalized human adenocarcinoma cell lines such as Caco-2 or T84.^{3–6} These cells are commonly grown on semi-permeable Transwell[®] inserts, where they form a polarized monolayer and exhibit microvilli formation. Despite many advantages such as easy cell culture and high reproducibility, these models have severe limitations in regards to properties required for a successful drug absorption test system. These limitations include for example, the lack of important mucus-secreting goblet cells and inconsistent expression of drug transporters and metabolic proteins depending on the culture conditions applied. In addition, tight junction formation between Caco-2 cells lead to an unusual tight barrier as exemplified by transepithelial electrical resistance (TEER) values greater than 300 Ωcm^2 .⁷ These TEER values are rather artificial high when compared to the native human small intestine with $\sim 40 \Omega\text{cm}^2$.⁸

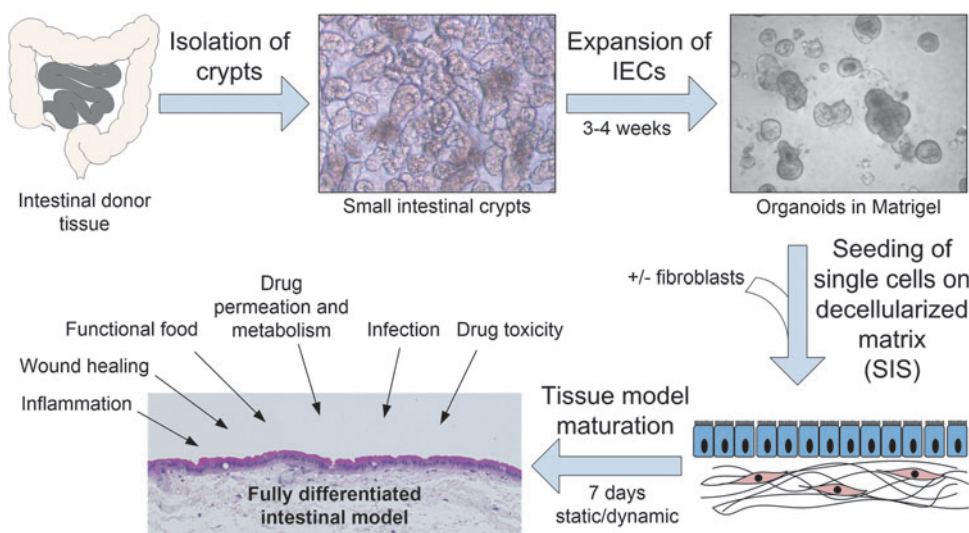
¹Department of Tissue Engineering and Regenerative Medicine (TERM), University Hospital Würzburg, Würzburg, Germany.

²Helmholtz Institute for Pharmaceutical Research Saarland (HIPS), Helmholtz Centre for Infection Research (HZI), Saarland University, Saarbrücken, Germany.

³Department of General, Visceral, Vascular and Pediatric Surgery, University Hospital of Würzburg, Würzburg, Germany.

⁴Translational Center Würzburg “Regenerative Therapies for Oncology and Musculoskeletal Diseases” (TZKME), Würzburg Branch of the Fraunhofer Institute Interfacial Engineering and Biotechnology (IGB), Würzburg, Germany.

FIG. 1. Schematic of primary intestinal tissue model established in this study. IECs were isolated from human small intestinal tissue and expanded as organoid culture for 3–4 weeks. After enzymatic digestion single cells were seeded on a decellularized biological scaffold (SIS) with or without intestinal fibroblasts. Tissue models were cultured for 7 days under static or dynamic conditions and can be used for various research applications (Illustration gut: Copyright©motifolio.com). IEC, intestinal epithelial cells; SIS, small intestinal submucosa. Color images available online at www.liebertpub.com/tec



Recent developments in terms of cultivating human primary intestinal epithelial cells (hIECs) enabled the development of novel, more *in vivo*-like organoid models.^{9,10} These organoids are small representatives in structure and function of the respective native organ. Adult intestinal (stem) cells directly isolated from human biopsies can be reliably propagated within this system for several months without significant changes in phenotype. Subsequently, these cells can then be reliably differentiated into the main intestinal cell types more closely mimicking the tissue development *in vivo*.⁹ However, the reduction of high costs and the complex handling of this kind of organoid culture still remain challenging. Moreover, such systems cannot be used to assess classical functionality that is typically determined in two-dimensional Transwell cultures.

Basic requirements, such as the formation of monolayers with tight junctions, intestinal permeability, and transport cannot be provided by the organoid culture.¹ To overcome some of these pitfalls, our study combines intestinal human primary organoids with a Transwell-like approach. Here, we cultivated organoid-derived cells on a decellularized natural matrix prepared from porcine gut (small intestinal submucosa [SIS]). The scaffold is composed of conserved extracellular structures and basal lamina components.¹¹ Such matrix resembles a much closer physiological 3D microenvironment and entails no additional barrier, which is of relevance especially for high-molecular test compounds or nanoparticles. Since shear stress and coculture with feeder cells have been shown to promote epithelial barrier function,^{11,12} we also integrated such advanced culture conditions in our primary Transwell-like tissue model. Taken together our model might provide a promising and reliable *in vitro* test system of the small intestine (Fig. 1).

Materials and Methods

Human tissue

Full-thickness jejunal tissues for hIECs and fibroblasts isolation were obtained from obese patients undergoing a stomach bypass operation at the surgery unit, of the University Hospital Würzburg ($n=6$, mean age 43.5 years, two male/four female). Informed written consent was obtained

beforehand and the study was approved by the Institutional Ethics Committee on human research of the Julius-Maximilians-University Würzburg (study approval number 182/10). The data were analyzed anonymously and according to the principles expressed in the “Declaration of Helsinki.”

Isolation and culture of human IECs and fibroblasts

IECs and fibroblasts were isolated from human full-wall gut resections, 10 cm² in size as described previously.^{9,13} Briefly, villi were scraped off the muscle-free mucosa using a sterile glass slide. The remaining tissue was transferred into a 50 mL falcon tube with 20 mL 4°C cold HBSS[−] (Sigma-Aldrich, St. Louis, MO), vortexed for 5 s and the supernatant discarded. This washing step was repeated until the supernatant was completely cleared of cell debris. Afterward, the tissue was incubated in 4°C cold 2 mM EDTA/HBSS[−] solution (Sigma-Aldrich, St. Louis, MO) for 30 min at 4°C under gentle rotation on a shaker. Subsequently, the tissue was washed once in 20 mL HBSS[−] by manually inverting the tube five times. The mucosa was transferred in a new tube with 10 mL HBSS[−] and manually shaken five times. This shaking procedure was repeated four times always using a new tube. Each cell fraction was checked for the amount and size of crypts within small drops under the microscope. The supernatants containing the most vital appearing crypts were pooled and centrifuged at 350 *g* for 3 min at room temperature (RT). Pellet was resuspended in 10 mL basal medium, DMEM-F12 Advanced (Invitrogen, Carlsbad, CA) supplemented with 1× N2, 1× B27, 1× Anti-Anti, 10 mM HEPES, 2 mM GlutaMAX-I (all from Invitrogen, Carlsbad, CA), 1 mM *N*-acetylcysteine (Sigma-Aldrich, St. Louis, MO), and the crypt number was estimated in a 10 μ L drop by microscopy. Crypts were centrifuged in a nonstick 1.5 mL tube at 350 *g* for 3 min at RT and the supernatant was removed. The tube with the cell pellet was placed on ice until further use. The pellet was resuspended in an appropriate amount of cold Matrigel[®] (Corning, Hickory, NC) that is, ~5000 crypts/mL. Drops of 50 μ L per well were seeded in a 24-well plate and incubated for 10–20 min until the Matrigel was well solidified. The culture medium contained a mixture of 50% fresh basal medium and 50% Wnt3A-conditioned medium.¹⁴ Furthermore, the following growth factors were added: 500 ng/mL hR-Spondin 1 (PeproTech, Rocky Hill, NY), 100 ng/mL

mNoggin (PeproTech, Rocky Hill, NY), 50 ng/mL mEGF (PeproTech, Rocky Hill, NY), 10 μ M Y-27632 (ROCK inhibitor; Tocris Bioscience, R&D Systems, Minneapolis, MN), 10 nM Gastrin ([Leu15]-Gastrin I; Sigma-Aldrich, St. Louis, MO), 10 mM Nicotinamide (Sigma-Aldrich, St. Louis, MO), 500 nM A83-01 (Tocris Bioscience; R&D Systems, Minneapolis, MN), 10 μ M SB202190 (Sigma-Aldrich, St. Louis, MO), 500 nM LY2157299 (Axon MedChem, Groningen, The Netherlands), and 500 μ L of this mixture was added per well. Organoids were harvested by resuspension of the Matrigel in 500 μ L of Cell recovery solution (Corning, Hickory, NC) per well and incubated for 1 h on ice. For single cell expansion, organoids were digested with TrypLE Express (Invitrogen, Carlsbad, CA) at RT for 10 min and seeded again in Matrigel with readjusted cell number of about 500 cells per Matrigel drop. Additionally, 10 μ M JAG-1 (Anaspec, Fremont, CA) and 10 μ M Y-27632 were added for the first 2 days. To enrich the stem cell population organoids were passaged every 5–7 days.¹

Subepithelial fibroblasts were isolated after IECs processing by digestion of the remaining connective tissue. Connective tissue was cut into small pieces with sterile scissors and transferred to a tube with 0.3 mg/mL Dispase II (Invitrogen, Carlsbad, CA)/0.25 mg/mL Collagenase Type XI (Sigma-Aldrich, St. Louis, MO) solution. After digestion for 30 min at 37°C the cells were centrifuged and the pellet resuspended in medium. Cells were cultured in FibroLife (CellSystems, Troisdorf, Germany) supplemented with 2% fetal bovine serum (Bio&Cell) and Anti-Anti (1 \times). Fibroblasts were used for Transwell-like models up to passage 5.

In vitro Transwell-like models

Primary models of the intestinal mucosa were prepared by seeding $8 \times 10^5/\text{cm}^2$ single IECs with or without $4 \times 10^5/\text{cm}^2$ fibroblasts on decellularized porcine gut scaffolds (SIS) fixed between two plastic cylinders, so-called cell crowns and cultured in 24-well plates at 37°C in the incubator. Seeded area of the 24-well format is 0.54 cm^2 per model. For SIS preparation, porcine jejunal segments were explanted from 6-week-old domestic pigs (Niedermayer, Dettelbach, Germany) and decellularized according to a standardized protocol published previously.^{15,16} Models were cultured for 7 days either under static conditions in a standard well plate, under dynamic conditions on an orbital shaker (OS, 77 rpm) or in a perfusion bioreactor (BR, flow rate: 3.8 mL/min). All models were initially kept in proliferation medium for 48 h under static conditions allowing cells to adhere. Afterward, medium was changed to differentiation medium, that is, reduction of Wnt3a-conditioned medium to 25% and no addition of nicotinamide and SB202190. Additionally, 10 μ M DAPT (*N*-[*N*-(3,5-Difluorophenyl)-L-alanyl]-*S*-phenylglycine *t*-butyl ester; Sigma-Aldrich, St. Louis, MO), a γ -secretase inhibitor to block Notch-signaling, was added to drive differentiation toward secretory lineage.^{17–19} Models were furthermore cultured either under static or dynamic conditions till day 7. The barrier integrity of the models was tested by measuring the TEER using a hand-electrode (Millicell ERS-2; Millipore, Billerica, MA) before the experiments. Complementary, FITC-dextran permeability assay (4 kDa) (Sigma-Aldrich, St. Louis, MO) was performed after the experiments. Only models with an *in vivo*-like TEER-value higher than $40 \Omega \text{ cm}^2$ (above cell-free scaffold) and FITC-dextran transport of $<2\%$

after 30 min were considered for analysis. For further analysis all tissue models were either fixed with 4% paraformaldehyde (PFA; Sigma-Aldrich, St. Louis, MO) or stored at -80°C in RLT plus lysis buffer (Qiagen, Hilden, Germany).

Design of culture systems and fluid dynamic simulation

The cell crown system and the bioreactor were designed to allow the culture of tissues at the interface between two separated fluid domains. For the design of tailored parts, SolidWorks 2014 x64 Edition (Dassault Systemes Deutschland GmbH, Stuttgart, Germany) was employed. Construction drawings were forwarded to GT Labortechnik (Arnstein, Germany) and parts were manufactured from polyether ether ketone (PEEK). To characterize the fluid dynamics, both culture systems were investigated by finite element method computations. Therefore, COMSOL Multiphysics (Comsol Multiphysics GmbH, Berlin, Germany) was employed. Geometry data were imported into the simulation software and the fluid domains were parameterized as water at a temperature of 37°C. Furthermore, the fluid density was set to 1005.5 kg/m^3 and the kinematic viscosity was set to $7.65 \times 10^{-3} \text{ Pa} \times \text{s}$. $V(\vec{x}, 0) = 0$ was set as initial condition, and no-slip conditions were assigned to all boundaries. For the bioreactor, additional inlet regions with a specific flow rate of $5.8 \text{ E}-8 \text{ m}^3/\text{s}$ and outlet region exhibiting ambient pressure conditions were defined. A normal stress boundary condition was set to the model's gas/liquid interface. Rotational fluid motion was induced by defining periodic volume forces of 1 Hz and 4 mm amplitude onto the cell culture medium in the cell crown system on the OS.

Histologic and immunofluorescence analyses

Tissue and scaffold samples were fixed with 4% PFA for 1 h at 4°C, processed for embedding in paraffin, and sectioned with a thickness of 5 μ m on a microtome (SM2010 R; Leica, Germany). Tissue slices were first deparaffinized with xylene and rehydrated in a graded series of ethanol according to standard protocols. Tissue and scaffold sections were stained with hematoxylin and eosin (H&E, Morphisto, Frankfurt am Main, Germany), Feulgen (Merck, Darmstadt, Germany), and Masson-Goldner trichrome (Chroma, Muenster, Germany) according to standard protocols for general morphological investigation.^{20–22} Further characterization of the models was done by immunofluorescence staining. Briefly, antigen retrieval was done by heat pretreatment at 100°C for 20 min in pH 6 citrate buffer (Roth, Karlsruhe, Germany). After blocking with PBS plus 0.3% Triton (Sigma-Aldrich, St. Louis, MO), 5% BSA (PanReac AppliChem, Darmstadt, Germany), and 5% donkey-serum (Biozol, Eching, Germany) for 30 min, slices were incubated with primary antibodies at 4°C overnight (Supplementary Table S1; Supplementary Data are available online at www.liebertpub.com/tec). After washing, anti-mouse/-rabbit-Alexa 555 and Alexa 647 secondary antibodies were added at a dilution of 1:400 in PBS for 1 h at RT. Samples were covered using Mowiol with DAPI (Sigma-Aldrich, St. Louis, MO) for staining of the nucleus. Analyses of all stainings were done by an inverted fluorescence microscope (Keyence BZ-9000, Japan). For ultrastructural analysis of tissue models by electron microscopy, samples were washed with 0.1 M PBS, fixed over night with 2.5% glutaraldehyde with ions at 4°C and stored in 50 mM sodium cacodylate (Sigma-Aldrich, St. Louis, MO) at 4°C.

Ultra-thin sections were prepared and processed for scanning or transmission electron microscopy (SEM and TEM).

RNA and DNA analyses

DNA was either extracted from native porcine gut tissue or the respective decellularized SIS using the DNeasy Blood & Tissue Kit (Qiagen, Hilden, Germany). DNA amount was determined using Quant-iT™ PicoGreen® dsDNA Assay Kit (Invitrogen, Carlsbad, CA) and normalized to the dry weight. Qualitative control was done by gel electrophoresis with 2% agarose gel. RNA was extracted from tissue samples using the RNeasy Micro Kit plus (Qiagen, Hilden, Germany) with a TissueLyser LT (Qiagen, Hilden, Germany) and following the manufacturer's protocol. iScript™ Reverse Transcription Supermix for real-time quantitative polymerase chain reaction (qPCR) was used to generate cDNA (Bio-Rad, CA). qPCR was carried out using a CFX 96 Real-time system with a C1000 Thermal Cycler (Bio-Rad, CA) and the Sso-Fast Eva Green Supermix (Bio-Rad, CA). The following reaction condition was chosen: 40 cycles of 95°C 10 s, 60°C 10 s, 72°C 30 s. Exon-spanning primer pairs were either selected from previous literature^{1,9,23,24} or self-designed using NCBI-Primer designing tool and manufactured by a supplier (Eurofins Genomics, Ebersberg, Germany) (Supplementary Table S2).

Transport studies

For evaluation of the epithelial transport properties, several standard reference substances were tested. All transport studies were performed at 37°C under static conditions, on an OS and in a flow-through bioreactor. Fluorescein sodium salt (Sigma-Aldrich, St. Louis, MO) as a low permeable substance was used to determine paracellular transport, propranolol hydrochloride (Sigma-Aldrich, St. Louis, MO) as a high-permeable substance for transcellular transport, and rhodamin123 (Sigma-Aldrich, St. Louis, MO) as substrate for the efflux-transporter *p*-glycoprotein (Mdr1). Reference substances were added in a volume of 300 µL basal medium to the apical compartment using following concentrations: 400 µg/mL fluorescein, 30 µg/mL propranolol, and 5 µg/mL rhodamin123. Samples (100 µL) of the basolateral lumen (total 900 µL) were taken between 0 and 120 min every 15 min and replaced with fresh medium. Quantitative analyses of fluorescein and rhodamin123 was determined by measurement of the fluorescence intensity using a microplate reader (Tecan; Infinite M200, Maennedorf, Switzerland). Propranolol concentration was analyzed by HPLC-MS/MS (Shimadzu Nexera LC-30AD, CTO-20AC with FCV-12AH, 8030 Plus; Shimadzu Corporation, Kyoto, Japan). The apparent permeability coefficient (Papp-value) was calculated for every substance.²⁵

Nanoparticle permeation studies

Poly(D,L-lactic-co-glycolic acid) (PLGA)-based nanoparticles (NPs) with an average size of 214 nm (Polydispersity index, PDI 0.05) were labeled with coumarin-6,²⁶ solved in a volume of 300 µL basal medium and added at a concentration of 1.0 mg/mL to the apical donor compartment of an intestinal mucosa Transwell-like system. Samples of 100 µL were taken basolaterally between 30 and 360 min every 30 min and replaced with fresh medium. To determine the quantitative

transport, the fluorescence intensity of coumarin 6-loaded NPs was measured with a Tecan microplate Reader Infinite M200 (Tecan; Maennedorf, Switzerland). Serial dilutions of the starting concentration of the NPs were used as standards to estimate the NP concentrations of the samples. For qualitative analysis by SEM (Supra 25, Carl Zeiss AG, Germany), basolateral solutions were centrifuged, washed twice with distilled water, dried on a glass slide, and sputtered with platinum. Intracellular uptake of NPs in IECs was confirmed by confocal microscopy with Leica TCS SP8 (Leica, Wetzlar, Germany).

Statistical analyses

Statistical analysis were performed with unpaired *t*-test with Welch's correction or with one-way ANOVA, Tukey's multiple comparison test. All statistical tests were done by GraphPad Prism 6 Software (GraphPad Software, Inc.). Results are given as mean ± standard deviation. The level of statistical significance is indicated as follows: **p* < 0.05, ***p* < 0.01, ****p* < 0.001. A *p*-value between 0.05 and 0.15 was additionally considered as moderate evidence for statistical significance and biological relevance (0.05 < [#]*p* < 0.15).

Results

The central goal of our study was to provide an improved intestinal test system, which includes the essential requirements to reflect the *in vivo* physiology. This comprises different primary epithelial cell types of the gut, subepithelial mesenchymal cells, extracellular matrix support, and physiological shear stress (Fig. 1). In the following we introduce the different components within individual sections.

Preparation of a biological scaffold (SIS) for gut tissue engineering

The intestinal model developed in this study includes a decellularized biological scaffold generated from porcine jejunum (Fig. 2). After the mucosa was mechanically removed, decellularization and gamma-sterilization, the obtained matrix macroscopically appeared completely whitish (Fig. 2B). Masson trichrome staining and SEM analysis visualized the largely preserved collagen fibers of the subepithelial connective tissue (Fig. 2C, D, and H). Feulgen staining and DNA isolation confirmed that no significant DNA residuals could be detected after the decellularization process (Fig. 2E, F, and H). This was also confirmed in a quantitative analysis by PicoGreen® dsDNA assay (mean 219 ng DNA per mg dry weight, *n* = 3).

Propagation of primary human intestinal epithelial cells

Human crypt-derived primary IECs, isolated from jejunum tissue were embedded in Matrigel allowing formation of intestinal organoid structures according to the protocol published by Sato *et al.* (Fig. 3A).¹⁰ These organoids contained the main differentiated cell types and undifferentiated, proliferating stem and progenitor cells in crypt niches indicated by immunostaining for the proliferation marker Ki67 (Fig. 3B). To provide enrichment of these proliferating cells, organoids were kept relatively small (size ~ 150–200 µm) and passaged every 5–7 days. For quantitative analysis cells were labeled with EdU, which is incorporated into the DNA during cell division.

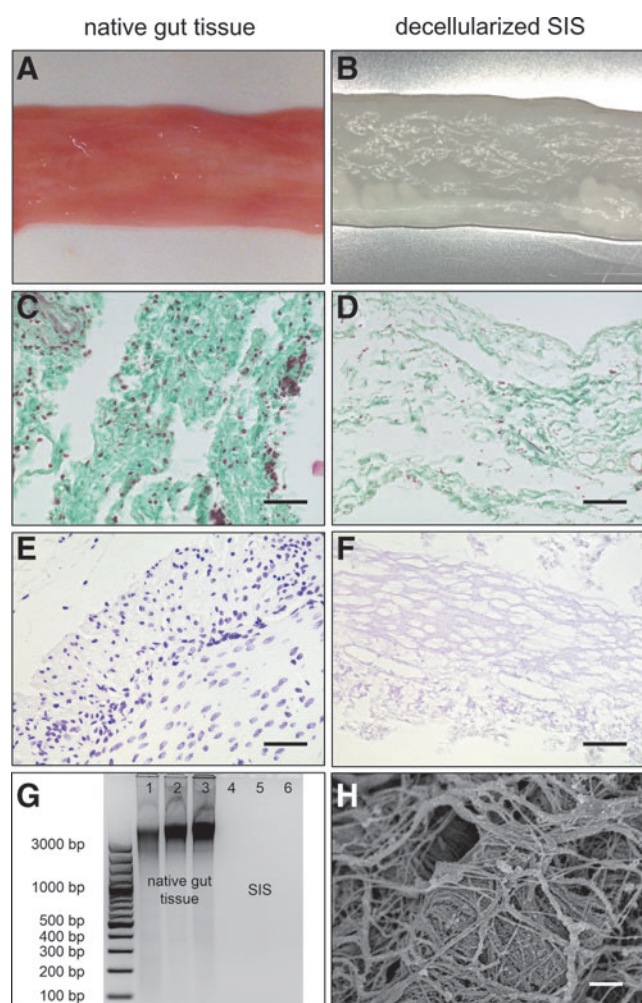


FIG. 2. Decellularized biological matrix (SIS) used for intestinal model. Visual control of porcine tissue before and after the decellularization process (A, B). Trichrome staining revealed a matrix of green stained collagen fibers, which were preserved during the process (C, D). Feulgen staining demonstrated that DNA of the porcine cells was completely removed (E, F). Qualitative agarose gel electrophoresis verified that there is no detectable DNA after the decellularization process of the SIS (G, lane 4–6). SEM analysis of the SIS revealed dense collagen fibers (H). Scale bar in (A–F) 20 μ m, in (H) 1 μ m. SEM, scanning electron microscopy. Color images available online at www.liebertpub.com/tec

Subsequent flow cytometry analysis demonstrated a large fraction of $\sim 29.5\%$ EdU-positive cells ($n=4$) (Fig. 2C).

Establishment of an intestinal Transwell-like in vitro model

IECs, propagated as organoids, were prepared as single cells and seeded on the decellularized SIS matrix up to 14 days under static culture conditions. Furthermore, we analyzed the biological effects of intestinal subepithelial fibroblasts on barrier integrity. HE-staining of the monoculture (Fig. 4A) demonstrated a confluent monolayer formation on top of the matrix after 5–7 days, which remained largely unchanged in terms of TEER and paracellular FITC-dextran transport during extended culture periods. Interestingly, coculture with fibroblasts led to a more heterogeneous monolayer with partly high prismatic cells and luminal cystic structures within the epithelium (Fig. 4B; black asterisk). The vimentin-immunostained fibroblasts were located directly underneath the E-cadherin-positive epithelium (Fig. 4C). The TEER-measurement revealed relatively low (compared to Caco-2 model) and no significantly different values between mono- and coculture (both $>40 \Omega \text{cm}^2$). The FITC-dextran permeability was much more robust (i.e., $\sim 1\%$ vs. 4% after 30 min) in the coculture compared to the monoculture (Fig. 4D, E) confirmed by significant differences between the variances of the two groups. Additionally, gene-expression analysis showed no significant differences neither in the goblet cell-specific Mucin 2 nor the tight junction-specific gene Claudin 4 between the mono- and the coculture (Fig. 4F). In contrast to organoids treated with DAPT, the Transwell-like cultures showed a fourfold reduction of Mucin 2 expression and 15-fold higher expression of claudin 4.

To prove the performance of our Transwell-like system for (pre-)clinical relevant NP uptake studies, we applied PLGA-NPs (1 mg/mL) with an average size of 214 nm over a time course up to 6 h. In contrast to an empty SIS, nanoparticles were first detected basolaterally after 1–2 h followed by a linear transport over time (Fig. 5A). After 6 h we detected about 5.5% transported NPs compared to the apically applied amount. Confocal imaging confirmed the uptake of the fluorescence-labeled NPs (green) into the cytosol of the IECs (Fig. 5B). To verify the actual particle transport through the cells and membrane, we performed SEM imaging on representative samples taken from the basolateral compartment after 6 h and detected particles (Fig. 5C).

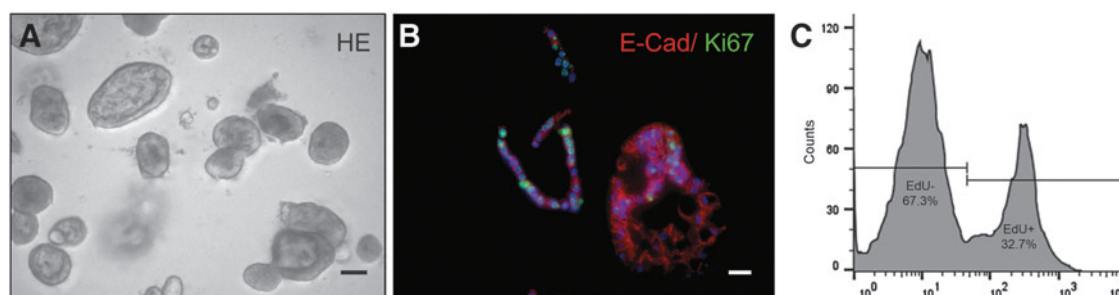


FIG. 3. Propagation of intestinal organoids. Intestinal epithelial cells growing as organoids embedded in Matrigel[®] (A). Immunostaining of organoids showed accumulation of proliferating cells positively stained for Ki67 (green nuclei; B). Quantification of proliferating cell population by flow cytometry revealed a population of 32.7% dividing cells (C). Scale bar in (A) 100 μ m, in (B) 20 μ m. Color images available online at www.liebertpub.com/tec

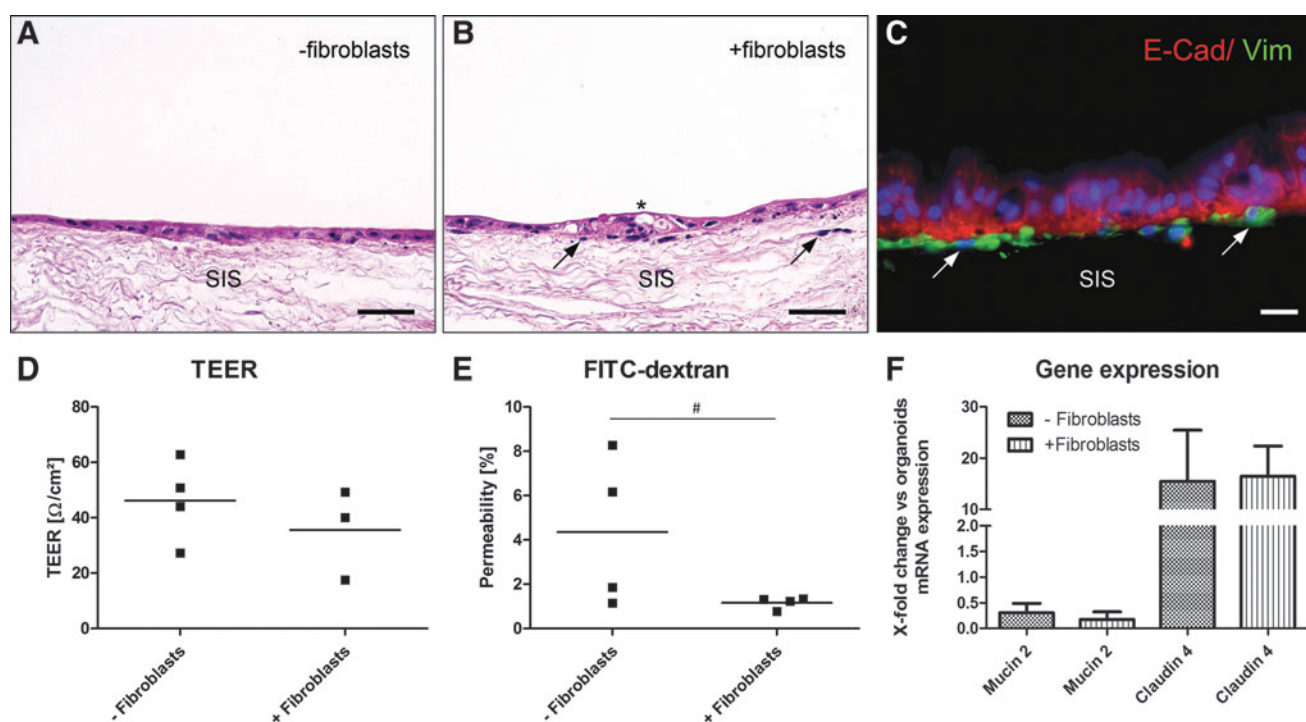


FIG. 4. Establishment of intestinal coculture on decellularized SIS. HE-staining of mono- and coculture shows a tight epithelial layer on top of the biological matrix (A, B, arrow: fibroblasts, star: inclusions). Immunostaining of epithelial cells (C; red: E-cadherin) and fibroblasts (C; arrow; green: vimentin). Transepithelial resistance is comparable between mono- and coculture (D; TEER) but FITC-dextran permeability was more robust in coculture (E). Statistical analysis showed only statistical trends for biological relevance in the mean value comparison ($^{\#}p < 0.11$), however, showed statistical significance in the comparisons of the variances of the two groups ($p < 0.0016$). The coculture revealed no differences in gene expression of Mucin 2 and Claudin 4, but differences of the Transwell® culture compared to organoids could be detected in either genes (F). Scale bar in (A, B) 40 μm , in (C) 20 μm ($n \geq 3$). TEER, transepithelial electrical resistance. Color images available online at www.liebertpub.com/tec

Influence of controlled dynamic culture conditions on intestinal Transwell-like culture

In vivo, intestinal cells are continuously exposed to shear stress and dynamic flow conditions. Therefore, we compared static, OS, and dynamic-bioreactor (BR) conditions. For the

static and OS setting we used cell crowns allowing fixation of membranes and culture in a standard 24-well format (Fig. 6A). For mechanical stimulation, scaffolds with cells were either placed on an OS (77 rpm) or within a bioreactor system (BR) allowing to apply defined, consistent shear stress to the tissue (Fig. 6B). For the BR, we chose a flow rate of 3.8 mL/min,

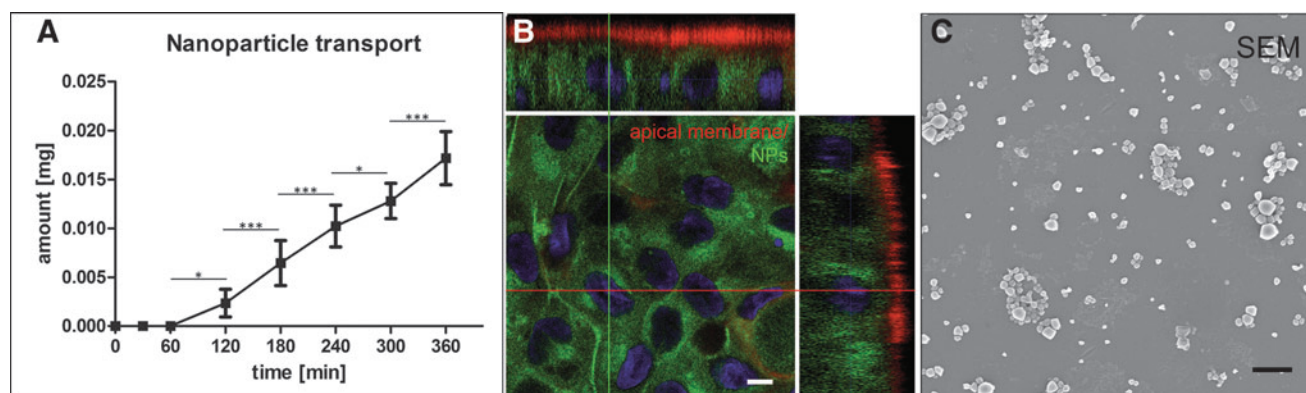


FIG. 5. Functional NP uptake studies. Linear transport of PLGA-NPs (1 mg/mL) was tested over a time period of 6 h and showed significant increase of particle transport after 120 min (A, $n = 3$). Confocal image showing NPs in the cytosol (green), the apical cell membrane visualized with CellMask™ Deep Red (red), and the cell nucleus with DAPI (blue) (B). SEM image of particles from the basolateral compartment after transport confirmed particles crossing the epithelial barrier (C). Scale bar in (B) 10 μm , (C) 1 μm . PLGA-NPs, poly(D,L-lactic-co-glycolic acid) nanoparticles; SEM, scanning electron microscopy. Color images available online at www.liebertpub.com/tec

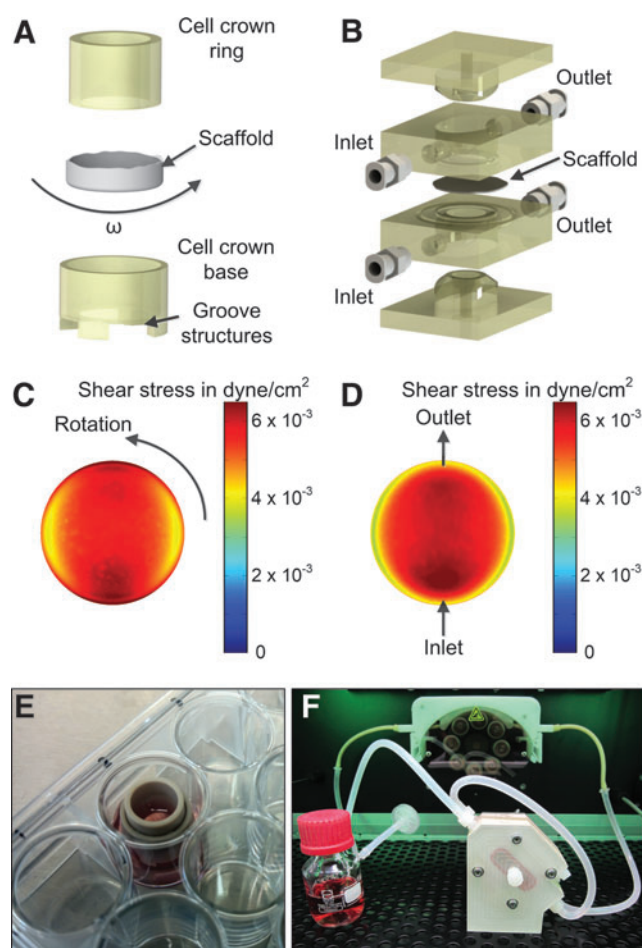


FIG. 6. Culture devices and fluid dynamic characterization. The cell crown system supported usage of a biological scaffold in a 24-well (A). The scaffold was clamped between the cell crown ring and the cell crown base. A fit ensured separation of inner and outer fluid domain. Convective flow was induced by a continuous rotational motion of constant frequency ω (1/s). Groove structures underneath the scaffold facilitated increased mass transport. A bioreactor system allowed dynamic culture conditions at the interface between two fluidic domains (B). Cell culture medium was pumped through each domain from the respective inlet to the outlet. Fluid dynamic simulations revealed a defined, consistent mechanical shear stress distribution on the scaffold surface in the cell crown system (C). The bioreactor design ensured reproducible mechanical stimulation (D). Except from a small outer ring, shear stress distribution showed low spatial variation across the scaffold surface. Image shows cell crown in 24-well plate format (E) and flow-through bioreactor in custom-designed incubator (F). Color images available online at www.liebertpub.com/tec

which has previously been proven as beneficial on intestinal differentiation.¹¹ Computational modeling demonstrated an average shear stress distribution of $7.1 \times 10^{-3} \pm 7.3 \times 10^{-4}$ dyne/cm² for the shaker (Fig. 6C) and $6.2 \times 10^{-3} \pm 1.0 \times 10^{-3}$ dyne/cm² for the bioreactor (Fig. 6D) across the scaffold surface. These values correspond well to mechanical stimulation found *in vivo* for the intestine.¹²

On a histological level, primary IECs cultured in the bioreactor (Fig. 7C) showed a more physiological high prismatic cell morphology (Fig. 7A–C). As mentioned, in

the static culture (Fig. 7A) fibroblasts remained directly under the epithelium; in contrast, on the shaker and bioreactor (Fig. 7B, C) cells also migrated into the matrix. On a transcriptomic level, applied culture conditions induced a fivefold downregulation of Mucin 2 compared to the organoids, while Claudin 4 expression was upregulated 6–15-fold, respectively (Fig. 7D). However, expression of the metabolic enzyme CYP3A4 and the important efflux transporter Mdr1 were significantly increased more than three-fold under the bioreactor conditions only (Fig. 7E, F).

For a functional proof of transport activity we furthermore applied typical reference substances with known transport properties. Fluorescein as a low permeable substance showed 3×10^{-6} cm/s higher P_{app} -values in the static and OS compared to the BR conditions with less than 1×10^{-7} cm/s, which lies below the Caco-2-model (dotted line) (Fig. 7G). Similar effects were observed for propranolol with P_{app} -values of about 6.5×10^{-6} cm/s, which is about 2×10^{-6} compared to the other conditions and more than five times lower than in the Caco-2-model (Fig. 7H). Instead, the ratio between basolateral-apical (b/a) and apical-basolateral (a/b) rhodamin 123 transport revealed a dramatically increased efflux transporter activity of more than 10-fold under the bioreactor conditions, which is comparable to the Caco-2-model (Fig. 7I).

Immunohistological characterization of the intestinal coculture model under optimized bioreactor conditions

In contrast to commonly used cell line models, the here developed primary model includes the main characteristic cell types also found in the small intestine *in vivo* as shown in a detailed histological analysis. Thus, the epithelial monolayer was not only positively immunostained for the general epithelial markers cytokeratin 18, pan-cytokeratin, and E-cadherin (Fig. 8A–F), but also for Mucin 1 and Mucin 2 (Fig. 8C, F; green: mucus-producing goblet cells) and Villin (Fig. 8B; green: absorptive enterocytes), which together represented the majority of cells in the monolayer. Furthermore, we detected also hormone-producing enteroendocrine cells immunopositive for chromogranin A (Fig. 8D; green) and paneth cells secreting lysozyme (Fig. 8E; green). These cells were identified as single cells equally distributed over the whole culture. SEM and TEM visualized a cell surface completely covered with microvilli (Fig. 8G, H). The ultrastructure analysis further confirmed tight-junction complexes and desmosomes at the cell–cell-border (Fig. 8H).

Discussion

Cell-line-based *in vitro* models such as Caco-2 are routinely used to investigate toxicity and uptake of orally delivered drugs.^{25,27,28} Despite many advantages, these models lack important gut characteristics including specific transporter activity and mucus production.²⁹ Therefore, previous research focused on developing primary human 3D models of the human small intestine, eventually leading to the primary gut organoid technique.¹⁰ However, standardized drug transport studies and infection studies are not feasible with organoid models.^{30,31} Meanwhile, a few primary Transwell-like barrier models with two separated compartments have been developed using various cell sources from ileum, rectum,¹ or other parts of small intestine³² using fetal,³³ postmortem tissue (MatTek) or unknown donor origin. Like

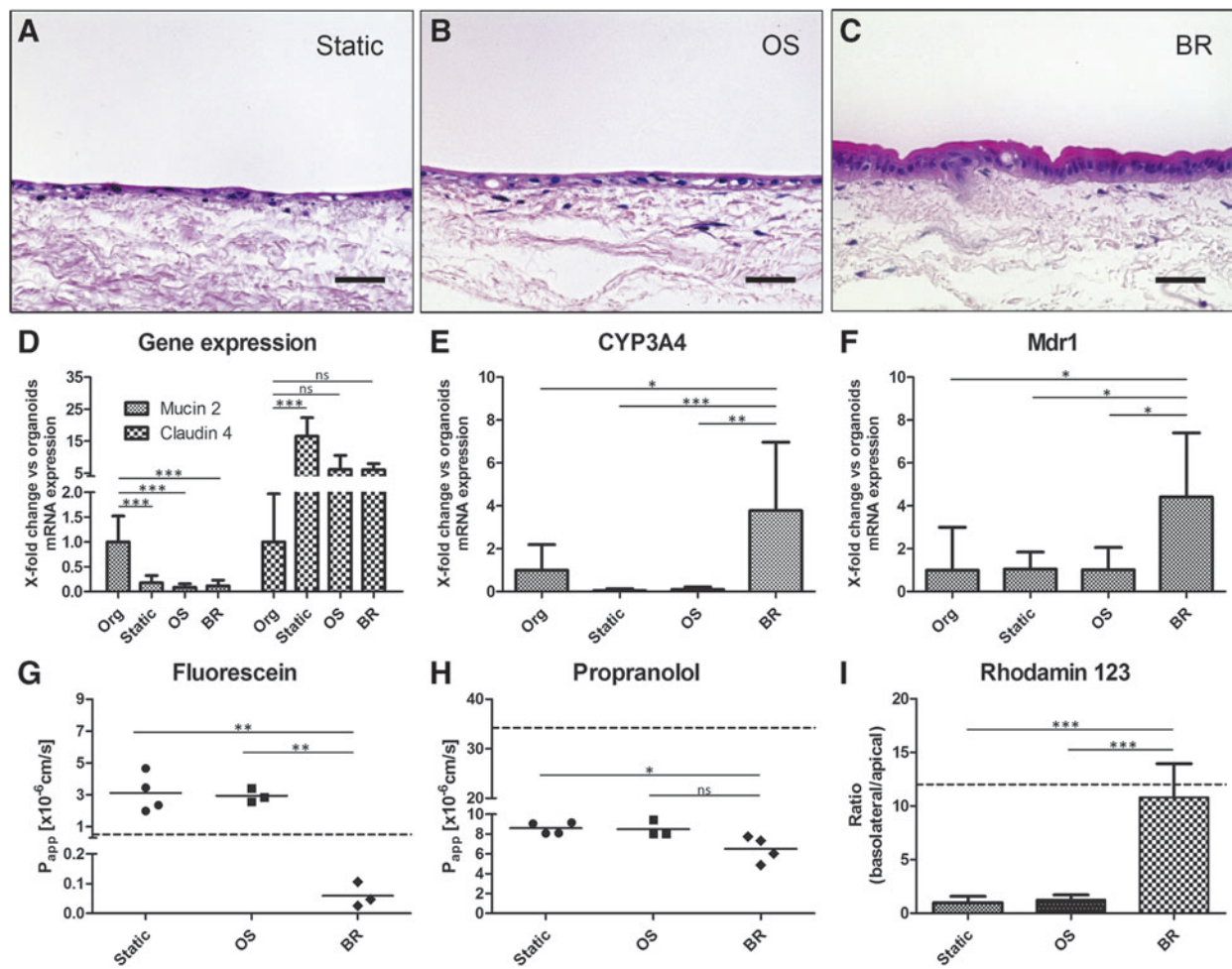


FIG. 7. Analysis of static compared to dynamic culture conditions on a shaker (OS) and in a bioreactor (BR). H&E staining of static culture (A), dynamic culture on shaker (B) and flow-bioreactor (C) shows differences in cell morphology and migratory potential of feeder cells into the matrix. Gene expression in monolayer cultures was reduced for Mucin 2 and induced for Claudin 4 compared to the organoids. Changes in gene expression between different culture conditions are particularly evident for CYP3A4 and Mdr1 under bioreactor conditions (E, F). Transport activity was tested by low-permeable fluorescein (G), high-permeable propranolol (H), and rhodamin123 as a substrate for the efflux transporter P-glycoprotein (I). In the bioreactor culture, fluorescein and propranolol showed notable slower transport; in contrast the efflux transporter activity was significantly higher as compared to the static and shaker culture. Dotted line shows P_{app} values for Caco-2 standard model according to Bock *et al.*⁴⁶ Scale bar: 20 μ m ($n \geq 3$). * $p < 0.05$, ** $p < 0.01$, *** $p < 0.001$. Color images available online at www.liebertpub.com/tec

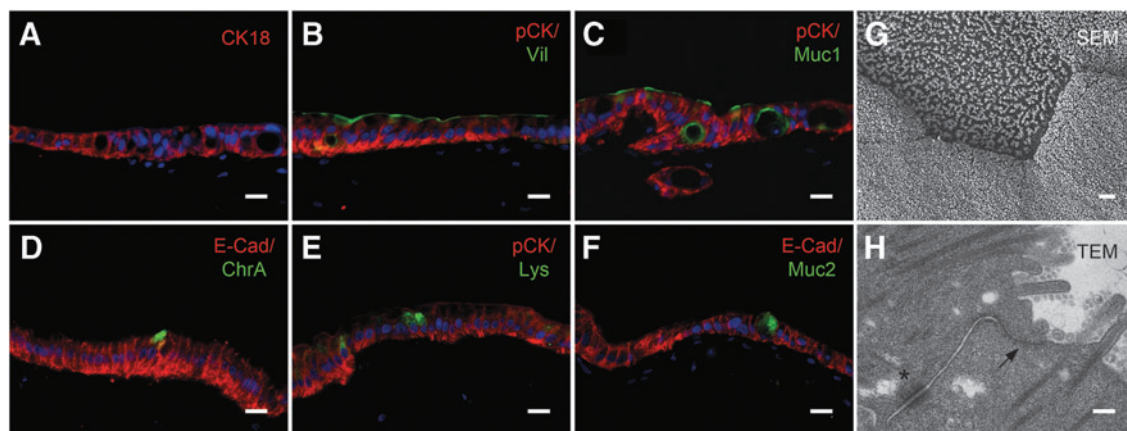


FIG. 8. Histological characterization of intestinal coculture model under bioreactor flow conditions. Immunohistological stainings of CK18 (Cytokeratin 18), pan CK, and E-Cad (E-cadherin) showed IECs (A–F) in combination with characteristic differentiation markers: Enterocytes (B; Villin), enteroendocrine cells (D; chromogranin A), paneth cells (E; Lysozyme), and goblet cells (C, F; Muc1/2). SEM (G) and TEM (H) image of epithelial cells indicate ultrastructural features such as microvilli, desmosomes (star), and tight junctions (arrow). Scale bar in (A–F) 20 μ m, in (G) 1 μ m, in (H) 200 nm. SEM, scanning electron microscopy; TEM, transmission electron microscopy. Color images available online at www.liebertpub.com/tec

Caco-2 assays these models also based on porous PET membranes as scaffold,^{1,32–34} which contain unequally distributed pores leading to impermeable areas and thus a significant artificial barrier for specific test formulations. This has been tested in a direct comparison of paracellular and transcellular drug transport after application on empty and Caco-2-seeded PET membranes or decellularized SIS.¹³ Similarly, PLGA nanoparticles designed for our study have been used in a (pre-)clinical trial and were transported much faster in our model compared to related studies using PET membranes.^{35,36} From literature it is known, that only 0.4–0.6%, of the encapsulated coumarin, is released over 5–48 h.^{37,38} That is why the percentage of false positive results within the uptake studies is lower than 1%. In addition to altered barrier properties, our decellularized porcine gut matrix (SIS) has been shown to promote (intestinal) cell differentiation,^{11,15,16,39} allows migration of coculture cells (e.g., fibroblasts) into the matrix, and needs no artificial coating with additional ECM components. In a previous more detailed characterization the matrix revealed a molecular structure mainly consisting of collagen type I fibers and smaller amounts of collagen type III, IV, and VI in addition to glycoproteins elastin, laminin, and fibronectin.⁴⁰ Cocultured fibroblasts can secrete important factors modulating epithelial cell behavior and signaling pathways such as Wnt,^{14,40} which could explain the more robust monolayer integrity observed in FITC-dextran transport. In particular, precise determination of the total Wnt-activity might help to fine-tune *in vivo*-like conditions in the future.⁴¹

TEER measurement provides a noninvasive method to ensure sufficient barrier integrity of the models before any experimental procedure.⁴² TEER-values measured in our model are in average about 40 Ωcm^2 , which is far below the Caco-2 model but in line with Ussing chamber TEER measurements using native human small intestinal tissue and previously published primary intestinal models.^{7,8,32,33} However, two other primary models also show higher TEER-values ranging between 130 and 900 Ωcm^2 , which could be caused by different donor tissues and culture protocols.^{1,34}

In our study, we also investigated the influence of mechanical stimuli, which have been shown to influence cell morphology and differentiation of cells.^{11,12,43–45} While the bioreactor applies a very good controlled and defined shear stress to the cells, inaccurate regulation, unequal movement, and waves can interfere with the system. The applied dynamic culture provided an average shear stress of 0.005 dyne/cm² to the cells, forces, which are in the range of physiological relevant values of about 0.002–0.08 dyne/cm² within the human intestine.¹² Despite the differences in viscosity of medium compared to the digested food, we could demonstrate biologically relevant effects of this approach. However, only the perfusion bioreactor lead to more physiological high-prismatic morphology, and increased expression of most important metabolic enzyme CYP3A4 and efflux transport Mdr1.⁴⁶ Furthermore, transport of low-permeable fluorescein⁴⁷ and high-permeable propranolol³³ was slower in the bioreactor setting and efflux transport of rhodamin123 increased comparable to values observed in the Caco-2-model.⁴⁸ In this respect, further functional validation using well-characterized reference compounds according to the FDA recommendations would be of interest.⁴⁹

In contrast to cell line models, our model comprises the cellular complexity of the different cell types found *in vivo*. In particular, mucus-producing goblet cells play an important role as the mucus layer poses an additional physical barrier and the first line of defence against pathogens.⁵⁰ Interestingly, chromogranin-producing enteroendocrine cells and lysozyme-secreting paneth cells can be also be found within the model. Further studies are necessary to fine balance the amount of different cell types within the gut epithelium *in vitro*.

In conclusion, we developed a human primary *in vitro* model of the small intestine representing the main physiological characteristics found *in vivo*. It might therefore be a promising tool for more predictive preclinical testings with pharmaceutical substances, probiotic active organisms, or human pathogenic germs. Finally, such a model could eventually help to reduce animal experimentations.

Acknowledgments

This study was funded by the BMBF (PeTrA, 13N11457). Prof. Dr. Georg Krohne (Division of Electron Microscopy; Biocenter of the University of Würzburg) kindly performed electron microscopy. We thank Mona Alzheimer (Research Center for Infectious Diseases, University of Würzburg) for proofreading the article.

Disclosure Statement

The authors disclose any commercial association that might create a conflict of interest in connection with the submitted article.

References

1. VanDussen, K.L., Marinshaw, J.M., Shaikh, N., Miyoshi, H., Moon, C., Tarr, P.I., Ciorba, M.A., and Stappenbeck, T.S. Development of an enhanced human gastrointestinal epithelial culture system to facilitate patient-based assays. *Gut* **64**, 911, 2015.
2. Maloy, K.J., and Powrie, F. Intestinal homeostasis and its breakdown in inflammatory bowel disease. *Nature* **474**, 298, 2011.
3. Sarmiento, B., Andrade, F., da Silva, S.B., Rodrigues, F., das Neves, J., and Ferreira, D. Cell-based *in vitro* models for predicting drug permeability. *Expert Opin Drug Metab Toxicol* **8**, 607, 2012.
4. Artursson, P., Palm, K., and Luthman, K. Caco-2 monolayers in experimental and theoretical predictions of drug transport. *Adv Drug Deliv Rev* **46**, 27, 2001.
5. Tran, Q.T., Gomez, G., Khare, S., Lawhon, S.D., Raffatellu, M., Baumler, A.J., Ajithdoss, D., Dhavala, S., and Adams, L.G. The *Salmonella enterica* serotype Typhi Vi capsular antigen is expressed after the bacterium enters the ileal mucosa. *Infect Immun* **78**, 527, 2010.
6. Raffatellu, M., Wilson, R.P., Chessa, D., Andrews-Polymenis, H., Tran, Q.T., Lawhon, S., Khare, S., Adams, L.G., and Baumler, A.J. SipA, SopA, SopB, SopD, and SopE2 contribute to *Salmonella enterica* serotype typhimurium invasion of epithelial cells. *Infect Immun* **73**, 146, 2005.
7. van Breemen, R.B., and Li, Y. Caco-2 cell permeability assays to measure drug absorption. *Expert Opin Drug Metab Toxicol* **1**, 175, 2005.

8. Sjöberg, Å., Lutz, M., Tannergren, C., Wingolf, C., Borde, A., and Ungell, A.-L. Comprehensive study on regional human intestinal permeability and prediction of fraction absorbed of drugs using the Ussing chamber technique. *Eur J Pharm Sci* **48**, 166, 2013.
9. Sato, T., Stange, D.E., Ferrante, M., Vries, R.G.J., van Es, J.H., van den Brink, S., van Houdt, W.J., Pronk, A., van Gorp, J., Siersema, P.D., and Clevers, H. Long-term expansion of epithelial organoids from human colon, adenoma, adenocarcinoma, and Barrett's epithelium. *Gastroenterology* **141**, 1762, 2011.
10. Sato, T., Vries, R.G., Snippert, H.J., van de Wetering, M., Barker, N., Stange, D.E., van Es, J.H., Abo, A., Kujala, P., Peters, P.J., and Clevers, H. Single Lgr5 stem cells build crypt-villus structures in vitro without a mesenchymal niche. *Nature* **459**, 262, 2009.
11. Pusch, J., Voteler, M., Gohler, S., Engl, J., Hampel, M., Walles, H., and Schenke-Layland, K. The physiological performance of a three-dimensional model that mimics the microenvironment of the small intestine. *Biomaterials* **32**, 7469, 2011.
12. Kim, H.J., Huh, D., Hamilton, G., and Ingber, D.E. Human gut-on-a-chip inhabited by microbial flora that experiences intestinal peristalsis-like motions and flow. *Lab Chip* **12**, 2165, 2012.
13. Lahar, N., Lei, N.Y., Wang, J., Jabaji, Z., Tung, S.C., Joshi, V., Lewis, M., Stelzner, M., Martín, M.G., and Dunn, J.C.Y. Intestinal subepithelial myofibroblasts support in vitro and in vivo growth of human small intestinal epithelium. *PLoS One* **6**, e26898, 2011.
14. Miyoshi, H., and Stappenbeck, T.S. In vitro expansion and genetic modification of gastrointestinal stem cells in spheroid culture. *Nat Protoc* **8**, 2471, 2013.
15. Linke, K., Schanz, J., Hansmann, J., Walles, T., Brunner, H., and Mertsching, H. Engineered liver-like tissue on a capillarized matrix for applied research. *Tissue Eng* **13**, 2699, 2007.
16. Schanz, J., Pusch, J., Hansmann, J., and Walles, H. Vascularised human tissue models: a new approach for the refinement of biomedical research. *J Biotechnol* **148**, 56, 2010.
17. Milano, J., McKay, J., Dagenais, C., Foster-Brown, L., Pognan, F., Gadiant, R., Jacobs, R.T., Zacco, A., Greenberg, B., and Ciaccio, P.J. Modulation of notch processing by γ -secretase inhibitors causes intestinal goblet cell metaplasia and induction of genes known to specify gut secretory lineage differentiation. *Toxicol Sci* **82**, 341, 2004.
18. van Es, J.H., van Gijn, M.E., Riccio, O., van den Born, M., Vooijs, M., Begthel, H., Cozijnsen, M., Robine, S., Winton, D.J., Radtke, F., and Clevers, H. Notch/[gamma]-secretase inhibition turns proliferative cells in intestinal crypts and adenomas into goblet cells. *Nature* **435**, 959, 2005.
19. Ogaki, S., Shiraki, N., Kume, K., and Kume, S. Wnt and notch signals guide embryonic stem cell differentiation into the intestinal lineages. *Stem Cells* **31**, 1086, 2013.
20. Fischer, A.H., Jacobson, K.A., Rose, J., and Zeller, R. Hematoxylin and eosin staining of tissue and cell sections. *CSH Protoc* **2008**, pdb.prot4986, 2008.
21. Chatelain, R., Willms, A., Biesterfeld, S., Auffermann, W., and Böcking, A. Automated Feulgen staining with a temperature-controlled staining machine. *Anal Quant Cytol Histol* **11**, 211, 1989.
22. Foot, N.C. The Masson trichrome staining methods in routine laboratory use. *Stain Technol* **8**, 101, 1933.
23. Burk, O., Arnold, K.A., Nussler, A.K., Schaeffeler, E., Efimova, E., Avery, B.A., Avery, M.A., Fromm, M.F., and Eichelbaum, M. Antimalarial artemisinin drugs induce cytochrome P450 and MDR1 expression by activation of xenosensors pregnane X receptor and constitutive androstane receptor. *Mol Pharmacol* **67**, 1954, 2005.
24. Wolbold, R., Klein, K., Burk, O., Nussler, A.K., Neuhaus, P., Eichelbaum, M., Schwab, M., and Zanger, U.M. Sex is a major determinant of CYP3A4 expression in human liver. *Hepatology* **38**, 978, 2003.
25. Artursson, P., and Karlsson, J. Correlation between oral drug absorption in humans and apparent drug permeability coefficients in human intestinal epithelial (Caco-2) cells. *Biochem Biophys Res Commun* **175**, 880, 1991.
26. Ma, W., Chen, M., Kaushal, S., McElroy, M., Zhang, Y., Ozkan, C., Bouvet, M., Kruse, C., Grotjahn, D., Ichim, T., and Mineev, B. PLGA nanoparticle-mediated delivery of tumor antigenic peptides elicits effective immune responses. *Int J Nanomed* **7**, 1475, 2012.
27. Yamashita, S., Tanaka, Y., Endoh, Y., Taki, Y., Sakane, T., Nadai, T., and Sezaki, H. Analysis of drug permeation across Caco-2 monolayer: implication for predicting in vivo drug absorption. *Pharm Res* **14**, 486, 1997.
28. Rubas, W., Cromwell, M.E., Shahrokh, Z., Villagran, J., Nguyen, T.N., Wellton, M., Nguyen, T.H., and Mersny, R.J. Flux measurements across Caco-2 monolayers may predict transport in human large intestinal tissue. *J Pharm Sci* **85**, 165, 1996.
29. Balimane, P.V., and Chong, S. Cell culture-based models for intestinal permeability: a critique. *Drug Discov Today* **10**, 335, 2005.
30. Mizutani, T., Nakamura, T., Morikawa, R., Fukuda, M., Mochizuki, W., Yamauchi, Y., Nozaki, K., Yui, S., Nemoto, Y., Nagaishi, T., Okamoto, R., Tsuchiya, K., and Watanabe, M. Real-time analysis of P-glycoprotein-mediated drug transport across primary intestinal epithelium three-dimensionally cultured in vitro. *Biochem Biophys Res Commun* **419**, 238, 2012.
31. Bartfeld, S., and Clevers, H. Organoids as model for infectious diseases: culture of human and murine stomach organoids and microinjection of *Helicobacter Pylori*. *J Vis Exp* November 12, 2015. DOI: 10.3791/53359.
32. Takenaka, T., Harada, N., Kuze, J., Chiba, M., Iwao, T., and Matsunaga, T. Human small intestinal epithelial cells differentiated from adult intestinal stem cells as a novel system for predicting oral drug absorption in humans. *Drug Metab Dispos* **42**, 1947, 2014.
33. Yamaura, Y., Chapron, B.D., Wang, Z., Himmelfarb, J., and Thummel, K.E. Functional comparison of human colonic carcinoma cell lines and primary small intestinal epithelial cells for investigations of intestinal drug permeability and first-pass metabolism. *Drug Metab Dispos* **44**, 329, 2016.
34. Kauffman, A.L., Gyurdieva, A.V., Mabus, J.R., Ferguson, C., Yan, Z., and Hornby, P.J. Alternative functional in vitro models of human intestinal epithelia. *Front Pharmacol* **4**, 79, 2013.
35. Roger, E., Kalscheuer, S., Kirtane, A., Guru, B.R., Grill, A.E., Whittum-Hudson, J., and Panyam, J. Folic acid-functionalized nanoparticles for enhanced oral drug delivery. *Mol Pharm* **9**, 2103, 2012.
36. Brito Baleeiro, R., Schweinlin, M., Rietscher, R., Diedrich, A., Czaplowska, J.A., Metzger, M., Michael Lehr, C., Scherließ, R., Hanefeld, A., Gottschaldt, M., and Walden, P. Nanoparticle-based mucosal vaccines targeting tumor-associated antigens to human dendritic cells. *J Biomed Nanotechnol* **12**, 1527, 2016.

37. Desai, M.P., Labhasetwar, V., Walter, E., Levy, R.J., and Amidon, G.L. The mechanism of uptake of biodegradable microparticles in Caco-2 cells is size dependent. *Pharm Res* **14**, 1568, 1997.
38. Panyam, J., Sahoo, S.K., Prabha, S., Bargar, T., and Labhasetwar, V. Fluorescence and electron microscopy probes for cellular and tissue uptake of poly(D,L-lactide-co-glycolide) nanoparticles. *Int J Pharm* **262**, 1, 2003.
39. Mertsching, H., Schanz, J., Steger, V., Schandar, M., Schenk, M., Hansmann, J., Dally, I., Friedel, G., and Walles, T. Generation and transplantation of an autologous vascularized bioartificial human tissue. *Transplantation* **88**, 203, 2009.
40. Shi, L., and Ronfard, V. Biochemical and biomechanical characterization of porcine small intestinal submucosa (SIS): a mini review. *Int J Burns Trauma* **3**, 173, 2013.
41. Schuijers, J., Junker, Jan P., Mokry, M., Hatzis, P., Koo, B.-K., Sasselli, V., van der Flier, Laurens G., Cuppen, E., van Oudenaarden, A., and Clevers, H. Ascl2 acts as an R-spondin/Wnt-responsive switch to control stemness in intestinal crypts. *Cell Stem Cell* **16**, 158, 2015.
42. Muendoerfer, M., Schaefer, U.F., Koenig, P., Walk, J.S., Loos, P., Balbach, S., Eichinger, T., and Lehr, C.-M. Online monitoring of transepithelial electrical resistance (TEER) in an apparatus for combined dissolution and permeation testing. *Int J Pharm* **392**, 134, 2010.
43. Shahin, K., and Doran, P. Shear and compression bioreactor for cartilage synthesis. In: Doran P.M., ed. *Cartilage Tissue Engineering*. New York: Springer, 2015, p. 221.
44. Rebelo, S.P., Costa, R., Silva, M.M., Marcelino, P., Brito, C., and Alves, P.M. Three-dimensional co-culture of human hepatocytes and mesenchymal stem cells: improved functionality in long-term bioreactor cultures. *J Tissue Eng Regen Med* 2015. [Epub ahead of print]. DOI: 10.1002/term.2099.
45. Jeong, S.I., Kwon, J.H., Lim, J.I., Cho, S.-W., Jung, Y., Sung, W.J., Kim, S.H., Kim, Y.H., Lee, Y.M., Kim, B.-S., Choi, C.Y., and Kim, S.-J. Mechano-active tissue engineering of vascular smooth muscle using pulsatile perfusion bioreactors and elastic PLCL scaffolds. *Biomaterials* **26**, 1405, 2005.
46. Paine, M.F., Hart, H.L., Ludington, S.S., Haining, R.L., Rettie, A.E., and Zeldin, D.C. The human intestinal cytochrome P450 “pie.” *Drug Metab Dispos* **34**, 880, 2006.
47. Berginc, K., Žakelj, S., Levstik, L., Uršič, D., and Kristl, A. Fluorescein transport properties across artificial lipid membranes, Caco-2 cell monolayers and rat jejunum. *Eur J Pharm Biopharm* **66**, 281, 2007.
48. Bock, U., Flototto, T., and Haltner, E. Validation of cell culture models for the intestine and the blood-brain barrier and comparison of drug permeation. *Altex* **21 Suppl 3**, 57, 2004.
49. Kratz, J.M., Teixeira, M.R., Koester, L.S., and Simões, C.M.O. An HPLC-UV method for the measurement of permeability of marker drugs in the Caco-2 cell assay. *Braz J Med Biol Res* **44**, 531, 2011.
50. McGuckin, M.A., Lindén, S.K., Sutton, P., and Florin, T.H. Mucin dynamics and enteric pathogens. *Nat Rev Micro* **9**, 265, 2011.

Address correspondence to:

Marco Metzger, PhD

Translational Center Würzburg “Regenerative Therapies for Oncology and Musculoskeletal Diseases” (TZKME)
Würzburg Branch of the Fraunhofer Institute Interfacial Engineering and Biotechnology (IGB)

Röntgenring 11

97070 Würzburg

Germany

E-mail: marco.metzger@igb.fraunhofer.de

Received: March 15, 2016

Accepted: July 29, 2016

Online Publication Date: August 22, 2016